Article

A Battery Capacity Configuration Method of a Photovoltaic and Battery System Applied in a Building Complex for Increased Self-Sufficiency and Self-Consumption

Shaojie Li, Tao Zhang, Xiaochen Liu and Xiaohua Liu *

Department of Building Science, Tsinghua University, Beijing 100084, China
* Correspondence: lxh@tsinghua.edu.cn; Tel.: +86-10-6277-3772

Abstract: Photovoltaic (PV) systems have been growing in popularity as an energy conservation and carbon reduction approach. Generally, battery storage is integrated with a PV system to solve the intermittent and fluctuant problems of solar resources, enhancing the relative independence of the PV–battery (PVB) system. In consideration of the economic benefits and system efficiency, it is necessary to investigate battery capacity allocation methods. A battery capacity configuration method was established in this study to increase the self-sufficiency rate (*SSR*) and self-consumption rate (*SCR*) of the system for a building complex by exploiting the battery resources. The PVB system designed for the building complex is divided into two categories: distributed and centralized storage. The *SSR* and *SCR* significantly increase with the increasing battery capacity for both schemes. The *SCR* of centralized storage is always higher than that of distributed storage, considering different battery and PV capacities. However, the *SSR* of distributed storage scheme was found to be slightly higher than that of the centralized storage scheme when the energy generated by PV is half of the energy consumed by the building load. For instance, when the battery capacity is four, *SSR* values for optimal distributed and centralized storage schemes are 47.62% and 47.19%, respectively. For the distributed storage scheme, there is a slight difference between the optimal allocation ratios achieved by *SSR* and *SCR*, considering that they have the same total battery capacity. In addition, the effects of converter loss, complementarity in load curves, and centralized batteries were analyzed to achieve greater *SSR* and *SCR*. The comparison results of this study can be used as a guide for battery capacity design in the PVB systems of building complexes.

Keywords: photovoltaic; battery capacity; building complex; self-sufficiency; self-consumption

1. Introduction

Recently, energy demand and carbon emissions have rapidly grown worldwide [1,2]. Building operations consume nearly 40% of the energy and generate approximately 30% of the total carbon emissions [3,4]. Renewable energy sources, which are sustainable, abundant, and convenient to use, are thought to be an alternative to traditional fuels [5]. Therefore, it is encouraged to take full advantage of clean, renewable energy sources. Solar power generation, wind power generation, and solar heat collection are common techniques [6]. The contribution of solar and wind energy to power generation is increasing and studies related to 100% renewable energy scenarios indicate that the contribution of solar PV may be more than 50% by 2050 [7]. The installed PV capacity in China increased from 0.03 GWh in 2009 to 204.18 GWh in 2019 [8].

Much attention has been paid to the distributed photovoltaic (PV) systems applied in buildings. By 2019, the U.S. had 70 GWDC of solar capacity and the National Renewable Energy Laboratory found that the technical solar potential of suitable residential buildings was over 700 GWDC [9]. Gul et al. [10] proposed a grid-connected PV system for a university campus and neighboring communities. The system exhibited excellent

performance in terms of flexibility, reliability, climate resilience, and carbon emission reduction. Gerber et al. [11] analyzed the efficiency of photovoltaics integrated with a DC power network in commercial buildings. The results indicated that buildings with large PV and battery capacities achieved efficiency savings of more than 11%. Ge et al. [12] investigated the matching characteristic of a rooftop hybrid photovoltaic–wind system and building energy consumption. The proposed general method for analyzing rooftop hybrid systems can enable widespread and efficient solar and wind energy utilization in densely populated urban areas. Zhang et al. [13] proposed a controller that achieved 12% annual electricity cost savings and 34% peak demand reduction for PV systems in commercial buildings compared with the baseline.

However, PV power generation fluctuates [14] and is intermittent [15] because of the solar source, which causes unstable and volatile electricity output to the grid [16,17]. Consequently, problems such as the curtailment of PV generation and difficulties in grid connection need to be urgently solved [18]. Configuration of the energy storage system is considered an effective way to solve these problems [19,20]. Generally, the chemical battery is chosen as the energy storage method, because of its characteristics of high energy density, long lifetime [21], and great performance in circulating operation [22]. Khezri et al. [23] evaluated the optimal sizing and economic analysis of a rooftop PV and battery energy storage system for grid-connected households. This study found that the PV–battery (PVB) system is more economical for all-electric houses. Argyrou et al. [24] proposed a novel power management strategy for a residential-grid-connected PV system with battery-supercapacitor storage to increase self-consumption and self-sufficiency. The system achieved effective power sharing among the PV, battery-supercapacitor storage, building load, and grid.

Despite the advantages of battery storage, its high cost [25] has been a significant obstacle in the deployment of chemical batteries in PV systems. It is necessary to investigate battery capacity allocation problems to achieve high system performance and economic benefits. Li et al. [26] developed a capacity optimization configuration method for a photovoltaic and energy storage hybrid system considering its entire life cycle. With the proposed capacity allocation method, the economic efficiency of the system was significantly improved while ensuring demand for the supply load. Zou et al. [27] discussed three groups of factors of uncertainty relating to outdoor conditions, building construction, and indoor conditions, in PV and battery capacity design. Capacity configuration indices were proposed to achieve the required self-sufficiency rate (*SSR*) and self-consumption rate (*SCR*) for office buildings in hot summer and cold winter areas. Li et al. [28] investigated the battery capacity that should be deployed to achieve a high load cover ratio of a grid-connected PVB system in gymnasium buildings. Mohamad et al. [29] optimized the battery capacity allocation for a PV power station and decreased the curtailment of the PV generation. Anuradha et al. [30] analyzed the effect of battery allocation on network loss and voltage variations in a distributed PV generation system with the goal of applicable power dispatch. Dawei et al. [31] proposed a novel battery capacity optimization configuration method that considers the rate characteristics in primary frequency regulation to enhance the power system frequency regulation capability and performance.

Most existing studies based on battery storage allocation in the PVB system have focused on the rooftop PV system of standalone buildings and large-scale PV power stations, even the integrated grid, aimed at price arbitrage, minimizing costs, improving grid frequency regulation, and improving power quality. Few studies have focused on the battery capacity configuration of building complexes comprising different types of buildings. The mismatch characteristics of the building load and PV generation for each building are diverse, which causes different battery capacities to be equipped in various buildings. When considering the building as a complex, both the power network topology and battery capacity allocation ratio influence the system performance. In this study, the appropriate battery configuration size and arrangement location were analyzed according to the *SSR* and *SCR*. This study attempted to reveal the differences between a single

building and a building complex in the battery size design phase. The main conclusions and contributions of this study are as follows:

(1)   A distributed storage scheme and centralized storage scheme of a building complex are proposed in this paper. The strengths of each scheme are compared based on the evaluation indicators.

(2)   The optimal allocation ratio of battery capacity with a distributed storage scheme is applied to the building complex.

(3)   A battery having a suitable size should be equipped to achieve high *SSR* and *SCR* for the centralized distributed scheme under different PV penetrations.

(4)   Evaluation criteria between *SSR* and *SCR* are selected while determining the battery configuration size of a building complex.

The remainder of this paper is organized as follows. In Section 2, the system layout and model of the components of the PVB system are presented. The evaluation indicators and operational strategy of the system are introduced. In Section 3, the process results of a single building, distributed storage scheme, and centralized storage are compared according to *SSR* and *SCR*. The effects of battery loss and converter loss on the indicators of the system are discussed in Section 4. In addition, the performance of the PVB system is analyzed for different PV penetrations. Finally, the relevant conclusions are presented in Section 5.

2. Materials and Methods

2.1. System Layout

Figure 1 shows the schematic design of the grid-connected PVB system for a single building, which comprises PV modules, battery, building loads, utility grid, DC/DC converters, and a bidirectional AC/DC inverter. The energy generated by the PV modules is supplied to the building load and battery, and it is exported to the utility grid when the PV electricity has a surplus. During PV shortage conditions, the battery is discharged and some energy is imported from the utility grid to guarantee electricity provision of the PVB system. The grid-connected PVB system for a building complex, composed of offices, apartments, and mall buildings, is displayed in Figure 2. All buildings are linked to a high-level DC bus using standalone DC/DC converters, and the energy exchange between the building complex and utility grid is achieved using a unified AC/DC inverter. Compared with the PVB system of a single building, there is an additional energy conversion process for building complexes considering a standalone DC/DC converter efficiency of 0.98. The configuration can be classified into two categories based on battery placement position. For the distributed storage scheme, the battery is linked to the DC bus of the building and provides service only for its buildings. In the centralized storage scheme, there are no battery banks in the building interior, and the battery is entirely arranged in the high-level DC bus, which is responsible for all buildings.
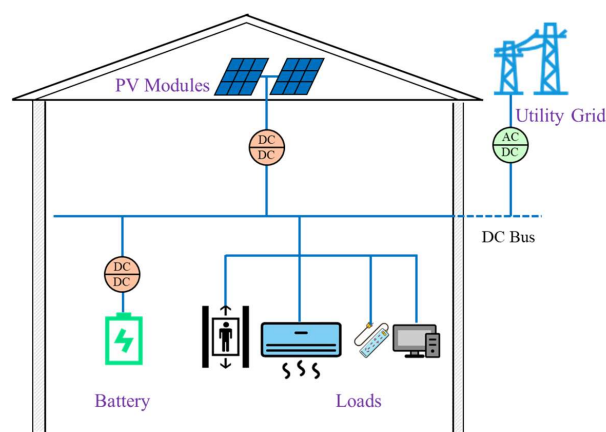

Figure 1. Topology of the grid-connected PVB system for a single building.
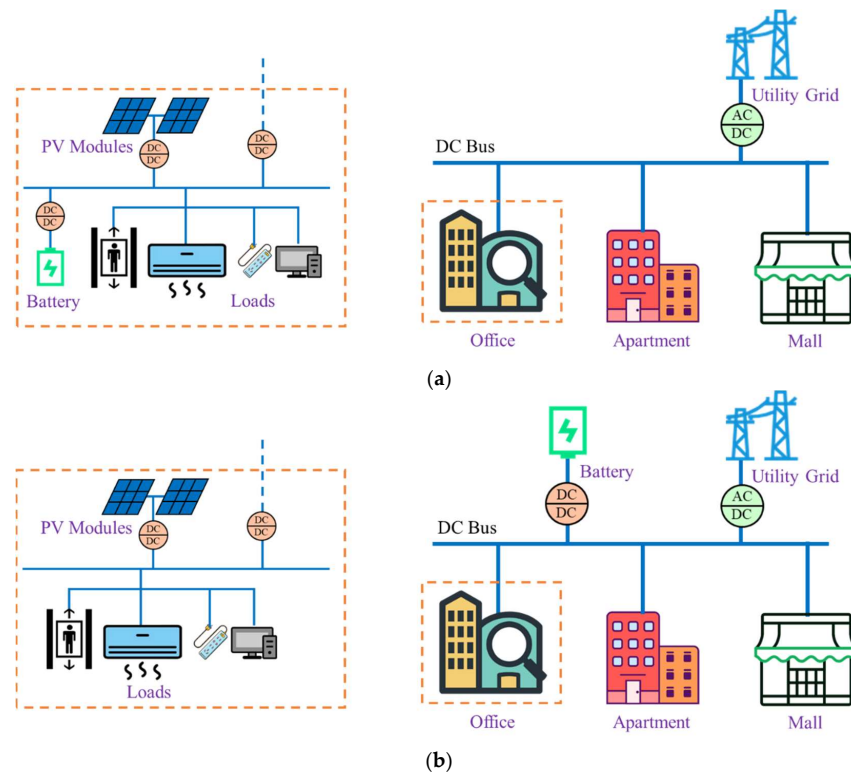
(a)

(b)

Figure 2. Topology of the grid-connected PVB system for a building complex: (**a**) distributed storage; (**b**) centralized storage.

Raw annual building load data were obtained from operating offices, apartments, and mall buildings in Beijing, China. For the convenience of load calculation and comparison, the load power time series of the three buildings were scaled to the same average daily electricity consumption of 100 kWh per day. In addition, the proportioned load profile was directly used as input power data during the simulation process. The detailed time series load data are illustrated in Appendix A.

2.2. System Model
2.2.1. PV Generation

The generation power of the PV system is determined as [32]:

$$P_{PV} = P_{PV,rated} \cdot \frac{I_t}{1000} [1 - \gamma \cdot (T_{PV} - 25)] \tag{1}$$

$$T_{PV} = T_a + \frac{I_t}{800} \cdot (NOCT - 20) \tag{2}$$

where P_{PV} indicates the actual generation power of the PV modules, $P_{PV,rated}$ indicates the rated PV generation power, I_t denotes the solar radiation intensity incident on the PV panels (W/m^2), γ symbolizes the temperature power coefficient (0.0045/°C), T_{PV} and T_a denote the temperatures of PV cells and ambient air, respectively, and *NOCT* indicates the nominal operating cell temperature (45 °C) [32].

The solar radiation intensity on the plane of the PV panels is calculated as [27]:

$$I_t = I_{dir}R_{dir} + I_{dif}\left(\frac{1 + \cos\beta}{2}\right) + I\rho\left(\frac{1 - \cos\beta}{2}\right) \tag{3}$$

where I_{dir}, I_{dif}, and I denote the direct solar radiation intensity, diffuse solar radiation intensity, and global solar radiation intensity on the horizontal plane (W/m^2), R_{dir} denotes the ratio of direct solar radiation on the inclined plane to the horizontal plane, ρ indicates

the reflectance coefficient of the ground (0.2), and β corresponds to the installation angle of the PV panels ($\beta = 30°$ is adopted in this study).

2.2.2. Battery System Model

The state of charge (*SOC*) is defined as the ratio of the energy content of the battery (E_b) to the rated battery capacity (Cap_b) in Equation (4). The operational conditions of the battery can be divided into charging and discharging processes as shown in Equation (5):

$$SOC = \frac{E_b}{Cap_b} \tag{4}$$

$$P_b = \alpha P_{b,ch} + (1 - \alpha)P_{b,dis} \tag{5}$$

where P_b denotes the actual operating power of the battery; $P_{b,ch}$ and $P_{b,dis}$ represent the charging power and discharging power of the battery, respectively; and α corresponds to a binary number, where 1 represents the battery charging process and 0 represents the battery discharging process.

The *SOC* is limited by the maximum and minimum states of energy (SOC_{max} and SOC_{min}) as shown in Equation (6). More specifically, P_b is limited by the maximum charging power ($P_{b,ch}^{max}$) and maximum discharging power ($P_{b,dis}^{max}$) to prevent over charging and over discharging, as shown in Equation (7):

$$SOC_{min} \leq SOC \leq SOC_{max} \tag{6}$$

$$P_{b,ch}^{max} \leq P_b \leq P_{b,dis}^{max} \tag{7}$$

During the discrete simulation process, *SOC* at each time step was calculated using Equation (8) [33]:

$$SOC(t + \Delta t) = SOC(t) - \alpha \frac{P_{b,ch} \cdot \Delta t \cdot \eta_{ch}}{Cap_b} - (1 - \alpha)\frac{P_{b,dis} \cdot \Delta t}{\eta_{dis} \cdot Cap_b} \tag{8}$$

where η_{ch} and η_{dis} denote the charging and discharging efficiencies of the battery, respectively; Δt symbolizes the time increment, and the time step is taken as 1/10 h in this study.

2.3. Evaluation Indicators

SSR and *SCR* were chosen as evaluation indicators of the PVB system in this study. *SSR* is the proportion of the total load consumption supplied by the PV-generated electricity. *SCR* is the proportion of the total PV generation consumed by the PVB system. Collectively, *SSR* and *SCR* denote the relative independence of the PVB system and utility grid, aimed at the supply and demand sides, respectively. *SSR* and *SCR* are defined in Equations (9) and (10), respectively:

$$SSR = \frac{E_{load} - E_{g,im}}{E_{load}} \times 100\% \tag{9}$$

$$SCR = \frac{E_{PV} - E_{g,ex}}{E_{PV}} \times 100\% \tag{10}$$

where E_{load} denotes the total electricity consumption of the building load (kWh), $E_{g,im}$ indicates the electricity imported from the utility grid (kWh), E_{PV} symbolizes the total electricity generated by the PV modules (kWh), and $E_{g,ex}$ indicates the electricity exported to the utility grid (kWh).

2.4. System Operation Strategy

For PVB systems, maximizing the *SSR* and *SCR* is usually the ultimate control goal, with the battery having the flexibility to charge and discharge. The system operation strategy is illustrated in Figure 3. For a single building, the battery is charged first when the PV generation has a surplus of energy, and is discharged when the PV generation is less

than the building load. The power of the battery is limited by the operational range of the *SOC* and maximum charging/discharging rate of the battery, as expressed in Equations (6) and (7). The power of the utility grid, building load, PV, and battery should maintain energy balance. Consequently, the power of the utility grid is calculated using the algebraic sum of the others. When distributed storage is adopted in the building complex, the battery control method for each building remains the same, except for the final exchange of power with the grid (P_g), which is calculated as the sum of P_g^i for each building, as determined by the system topology shown in Figure 2. For centralized storage, there is no battery inside the building, and the building achieves an electricity exchange with the DC bus. Hence, the unified battery will respond following the complementation of each building. For example, when the PV generation is larger than the office building load and the PV generation of the apartment cannot cover the building load, the battery is probably not charged or discharged because of the demand and supply offset in the two buildings. The operating state of the battery is determined by the total energy requirement of the buildings and the battery safety management limit, as shown in Figure 3.
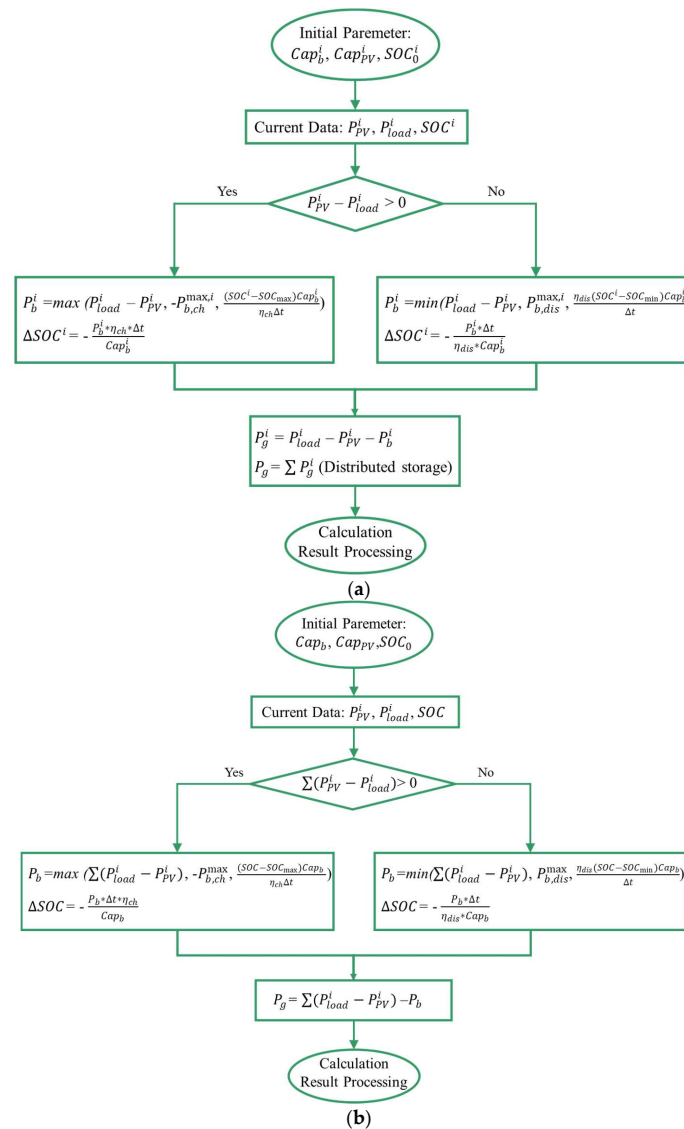

Figure 3. Flow chart of the system strategy (the superscript i represents office, apartment, and mall): (**a**) single building and distributed storage (the power of utility grid is the algebraic sum of P_g^i for three buildings); (**b**) centralized storage.

3. Results

The total PV energy generation during the entire year is the same as the annual building load for offices, apartments, and malls. For the convenience of comparison of battery capacity for different buildings, the battery is nondimensionalized by a multiple of the average daily building load (100 kWh). The detailed specifications of the battery bank used in this study are listed in Table 1 [18].

Table 1. Specification of the battery used in this study.

Parameters	Value
$SOC_{\max}$	0.95
$SOC_{\min}$	0.1
Max charging/discharging rate ($Rate_b$)	0.5 C
η_{ch}/η_{dis}	95%
Cycle times	6000
Service life	15 years

3.1. Single Building

The effect of battery capacity in a single building on *SSR* and *SCR* is discussed in this section. The results are illustrated in Figure 4. For each type of building, both *SSR* and *SCR* significantly increase with the increasing battery capacity. The increasing trend slows when the battery capacity is relatively high. This indicates that a greater Cap_b can increase the independence of the PVB system in terms of both self-sufficiency and self-consumption. With the same battery capacity, the *SSR* and *SCR* of the apartment are the lowest compared to those of the office and mall. When Cap_b is lower than 0.8, the *SSR* and *SCR* of the mall are higher than those of the office. When the Cap_b is greater than 0.8, the *SSR* and *SCR* of the mall are lower than those of the office, and the difference gradually increases with an increase in Cap_b. For example, when Cap_b is equal to 0.2, *SSR* values for office, apartment, and mall are 0.62, 0.48, and 0.63, respectively. When Cap_b is equal to 2.0, *SSR* values for office, apartment, and mall are 0.82, 0.78, and 0.81, respectively. Table 2 lists the detailed battery capacities for each building under specific *SSR* and *SCR* values, which will be used as basic input data in the calculation in a later section.
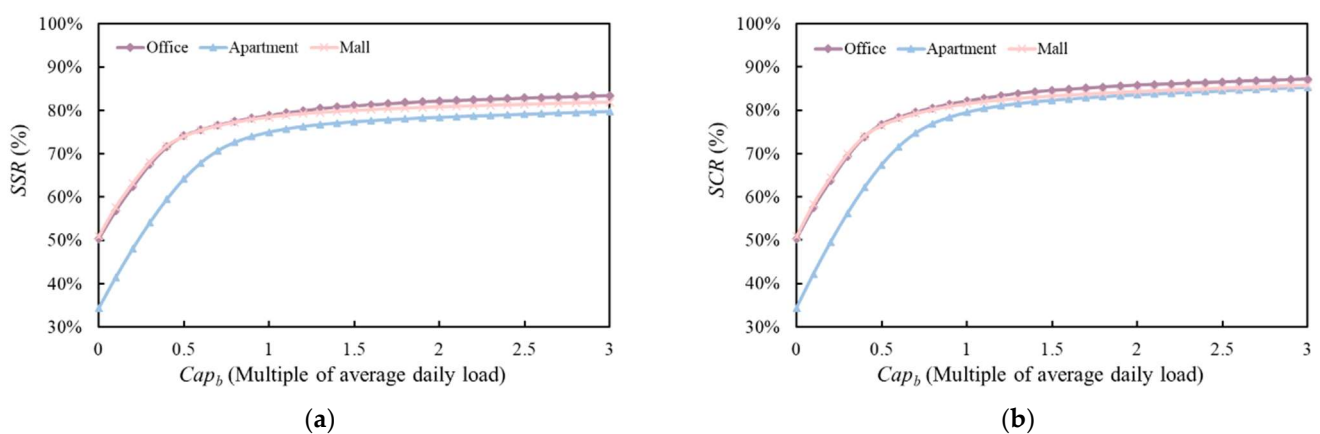

(**a**)　　　　　　　　　　　　　　　　　　　　　　　　　(**b**)

Figure 4. Evaluation indicators of the single building for different battery capacities: (**a**) *SSR*; (**b**) *SCR*.

3.2. Building Complex

3.2.1. Distributed Storage

In this section, the battery is placed inside the building and is not shared with others, as shown in the topology in Figure 2a. This implies that the battery allocated to each building will only absorb the surplus PV power generated inside the building and cover its load. However, the building complex is identified as a whole when calculating the

evaluation indicators. The effect of the proportion of battery capacity allocated among these buildings on the relative independence of the building complex with a certain total battery capacity is analyzed and not limited to a single building.

Table 2. Battery capacities for every single building under specific *SSR* and *SCR* values.

SSR	Cap_b				*SCR*	Cap_b			
	Office	Apartment	Mall	Sum		Office	Apartment	Mall	Sum
55%	0.070	0.316	0.058	0.444	55%	0.063	0.281	0.052	0.396
60%	0.156	0.410	0.141	0.707	60%	0.139	0.361	0.126	0.626
65%	0.249	0.520	0.237	1.006	65%	0.222	0.452	0.210	0.884
70%	0.358	0.670	0.346	1.374	70%	0.313	0.558	0.302	1.173
75%	0.553	0.994	0.568	2.115	75%	0.432	0.709	0.432	1.573
80%	1.188	2.993	1.452	5.633	80%	0.746	1.046	0.782	2.574
					85%	1.663	2.784	2.436	6.883

The battery capacity for each building is arranged according to the calculation results listed in Table 2 as the basic case, and the PVB system used the same evaluation indicators for the single building scheme. Figure 5 shows the concrete allocation capacity for each scenario and the corresponding *SSR* and *SCR* results. As shown in Figure 5, the gray dashed line represents the reference indicators of the original single-building scheme. *SSR* of the basic case is less than the reference value, and the difference gradually decreases with an increase in battery volume. *SCR* of the basic case is greater than the reference value, and the difference gradually decreases with an increase in battery volume. As shown in Figures 1 and 2a, there is an additional DC/DC converter for each building in the distributed storage scheme for the building complex. The extra energy loss produced in this DC/DC converter requires the added electricity to be imported from the utility grid and the reduced electricity to be exported to the utility grid. Consequently, the *SSR* of the distributed scheme is lower than the reference value of the single building, and the *SCR* of the distributed scheme is higher than the reference value of the single building. The impact of the increased battery capacity can be explained by the fact that energy exchange is more likely to finish inside the building, and less energy is exchanged with the DC bus through the DC/DC. Therefore, the influence of the DC/DC loss weakens.
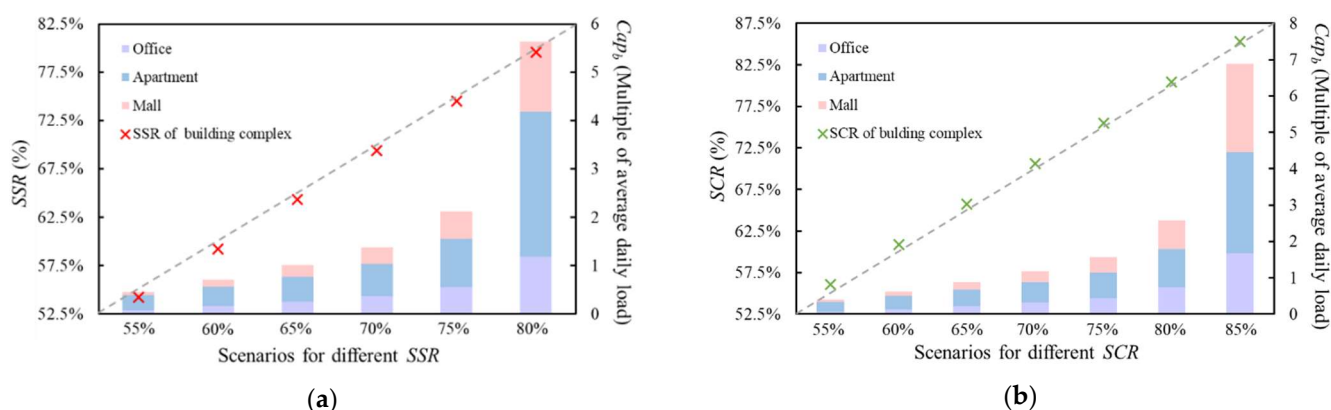

Figure 5. Results for the basic case with the same battery allocation determined by single building: (**a**) *SSR*; (**b**) *SCR*.

As mentioned above, the battery capacity allocated to each building influences the final *SSR* and *SCR* of the building complex. The optimal allocation to achieve the maximum *SSR* and *SCR* is discussed. The calculation patterns for all the allocation proportions are shown in Figure 6. The white marks correspond to the maximal *SSR* and *SCR* and the corresponding allocation ratio. For instance, when *SSR* reaches a maximum of 69.9%, the

capacity allocated for office, apartment, and mall is 0.413, 0.609, and 0.378, respectively. *SCR* reaches a maximum of 73.7% when the capacity allocated for the office, apartment, and mall is 0.413, 0.609, and 0.378, respectively. Using the optimization method shown in Figure 6, the optimal allocation proportion and maximum indicators under different battery capacities are acquired. As shown in Figure 7, the *SSR* and *SCR* of the building complex increase with an increase in total battery capacity. The battery is mainly dispatched to the apartment, particularly in the relatively low Cap_b situation, and the proportions for the office and mall are almost the same. This is determined by the characteristics of the relative independence of the PVB system in a single building, as discussed in Section 3.1. *SSR* and *SCR* of the apartment are the lowest of the three buildings, and *SSR* and *SCR* for the office and mall have almost no difference. Moreover, the allocation ratio comparison between Figures 7a and 7b indicates that the optimization directions of *SSR* and *SCR* are coincident, which means that the PVB system in a distributed storage scheme usually achieves a high *SCR* when the *SSR* of the system is high.
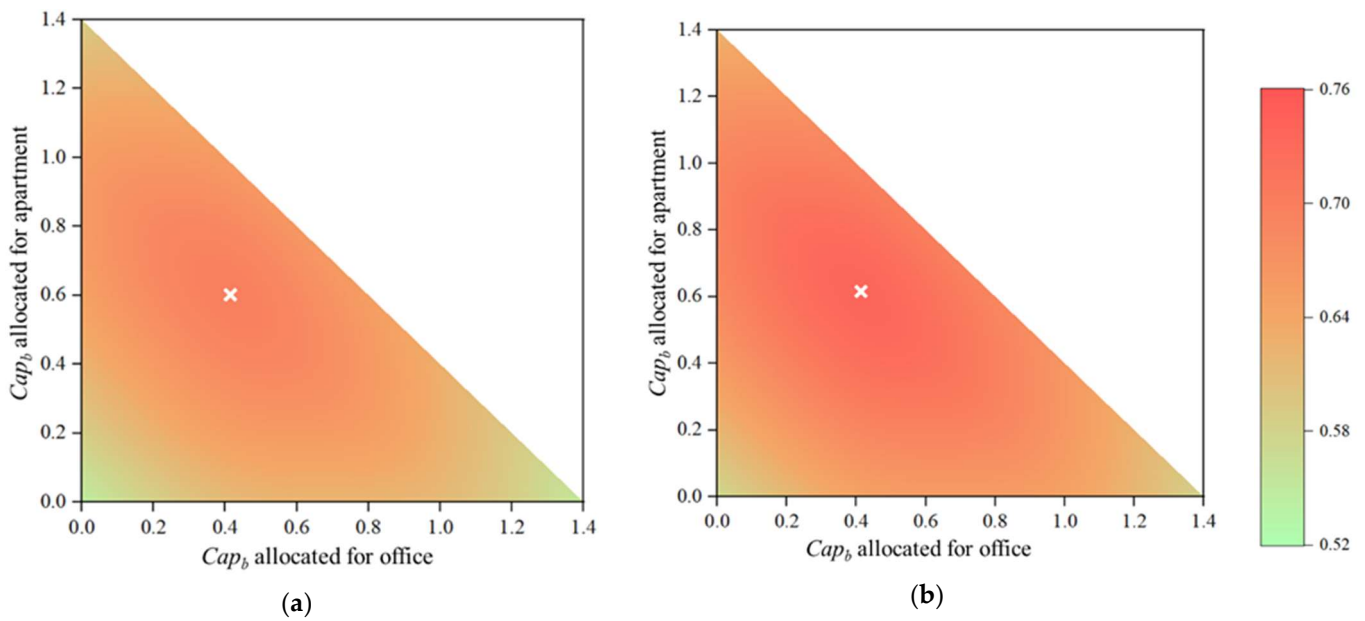

(**a**)　　　　　　　　　　　　　(**b**)

Figure 6. Optimal allocation processing pattern when Cap_b takes 1.4: (**a**) *SSR*, (**b**) *SCR*.
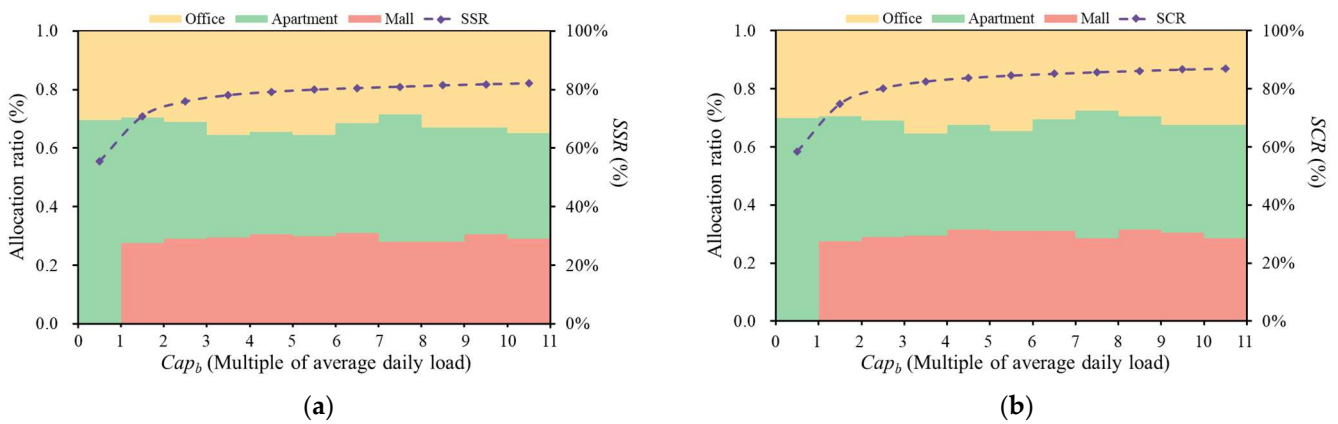

(**a**)　　　　　　　　　　　　　(**b**)

Figure 7. Allocation proportion and maximum indicators under different battery capacities: (**a**) *SSR*; (**b**) *SCR*.

3.2.2. Centralized Storage

The building complex adopts a centralized storage scheme with the topology shown in Figure 2b. There is only one battery location for the system, and Figure 8 analyzes the effect

of Cap_b on the two indicators. The green points indicate the results for the total capacity listed in Table 2. *SSR* and *SCR* of the building complex increase with total battery capacity.
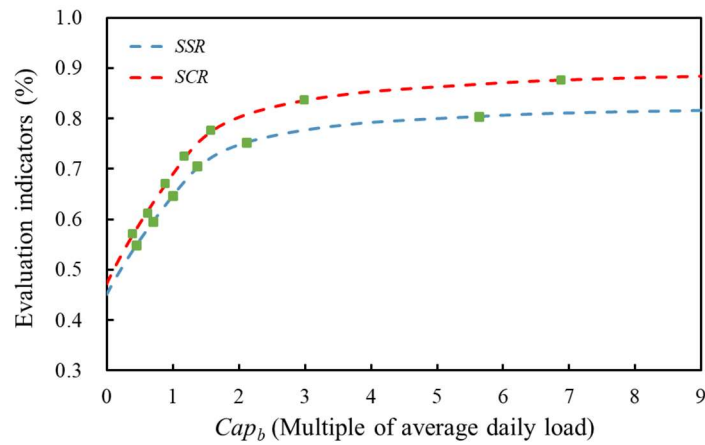

Figure 8. Calculation results of the centralized storage scheme for different battery capacities.

3.3. Comparison of Different Configuration Way

　　Figure 9 presents the comparison results of different battery arrangement schemes with the same total battery capacity aimed at different contrastive indicators. It can be observed from the title of the horizontal axis that the total battery capacity is chosen as the result in Table 2. For both *SSR* and *SCR*, the calculation results of centralized storage are maximal, and the results of the optimal allocation case are higher than those of the basic case. The *SSR* and *SCR* values of the horizontal axis are the results of a single building as a reference value. When Cap_b is 0.444, the *SSR* is lower than the reference value, which is caused by the energy loss of the converter. The difference gradually turns from negative to positive as Cap_b increases, which demonstrates the regulating effect of the battery. For *SCR*, the indicators of the three schemes are all higher than the reference *SCR*. Moreover, the difference between the optimal allocation case and reference *SCR* value decreases with an increase in Cap_b but gets larger for the centralized scheme and reference *SCR* value. This is mainly because a centralized battery can be utilized more adequately. In summary, the results imply that the centralized storage scheme is better for achieving the maximal *SSR* and *SCR*. The advantage of the centralized storage scheme increases with higher battery capacity.
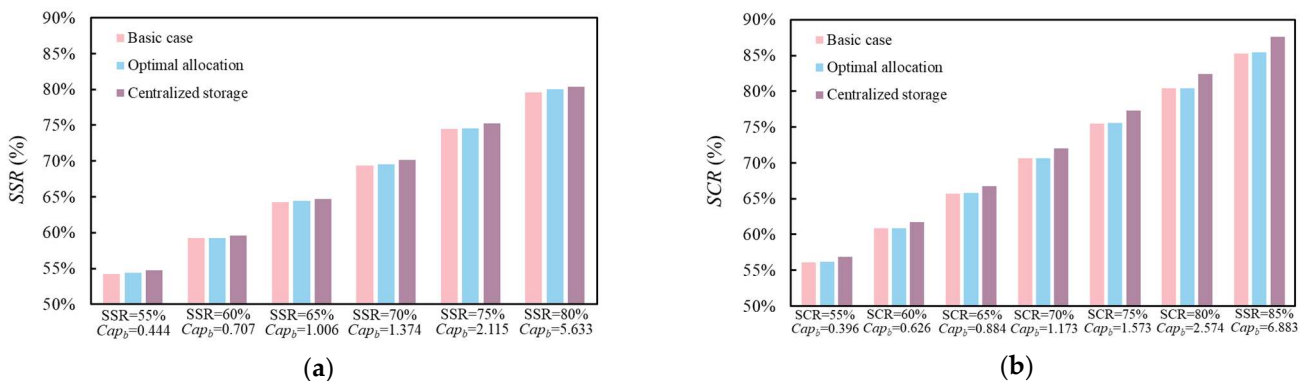

Figure 9. Comparison of different battery arrangement schemes: (**a**) *SSR*; (**b**) *SCR*.

4. Discussions

4.1. Energy Loss

　　The energy loss of the PVB system comprises battery loss and converter loss. Battery loss is generated during the charging and discharging processes as determined by η_{ch} and

η_{dis}. The converter plays a crucial role in the electricity transfer part of the PVB system. In particular, for a building complex, the DC/DC converter is responsible for linking the building itself and the entire DC system. Electricity losses occur in power electronic devices during the energy conversion process. This means that the greater the interaction between the building and high-level DC bus, the greater the converter loss.

Figure 10 shows the energy loss of the battery and converter corresponding to the case shown in Figure 9. The converter loss of the building complex is obvious compared to that of a single building. The converter loss of the basic case and optimal allocation decreases with an increase in Cap_b and the converter loss of centralized storage remains constant, as determined by the system control strategy depicted in Figure 3. The converter losses of the basic case and the optimal allocation are both lower than those of centralized storage. Converter loss requires more energy to be imported from the utility grid and less energy to be exported to the utility grid. Therefore, converter loss causes a decreased *SSR* and an increased *SCR*. The battery losses of these four scenarios are close in value, and the loss increases with an increase in Cap_b. A larger battery loss means that the battery is used more adequately and more energy is transported by the battery. Hence, as explained in Section 3.1, the effect of the battery will increase *SSR* and *SCR*, which will increase with an increase in battery capacity. As mentioned above, it is comprehensible that the *SSR* of the building complex is first lower than the reference, and the higher than the reference later; the *SCR* of the building complex is consistently higher than the reference, with the interaction of converter loss and battery. The total energy loss of centralized storage is the largest among the four scenarios, which proves that the *SCR* of centralized storage is maximal. However, this seems to conflict with the maximal *SSR* value of the centralized storage. This complementarity in the net electricity consumption curve of the three buildings improves the self-sufficiency of the system. The influence of complementarity is hidden by converter loss.
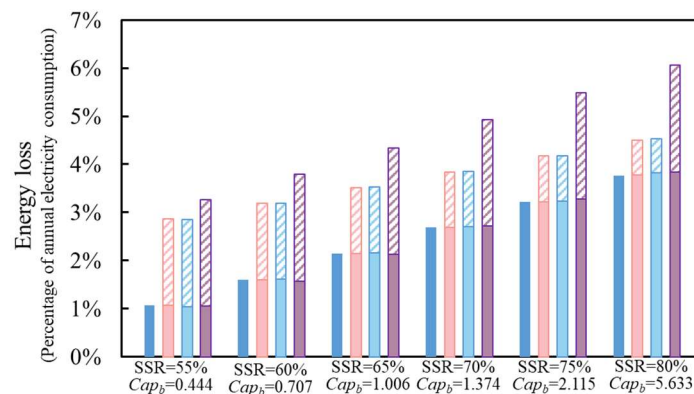

Figure 10. Analysis of energy loss under the same total battery capacities.

To explore the positive effect hidden by converter loss, the calculation results without considering converter loss are listed in Tables 3 and 4. The battery capacity of the system is arranged according to the results in Table 2 and matched with the relevant indicators. The *SSR* of distributed storage is higher than the corresponding reference value, and the *SSR* of centralized storage is higher than the *SSR* of distributed storage. This illustrates the effect of complementarity on net load curves. The electricity required from the utility grid may decrease under the condition that energy is surplus for one building but deficient for another, which shows a complementarity process without considering converter loss. For the distributed storage scheme, the net load curve of each building becomes smoother with a higher battery capacity, and the complementarity effect consequently weakens. Therefore, the difference between the *SSR* of the distributed storage and the reference value decreases with increasing battery capacity. For the centralized storage scheme, the net load curves of the three buildings are fixed, and the complementarity effect between the curves is constant. The difference between the *SSR* of distributed and centralized storage presents an

upward trend with increasing battery capacity. It is reasonable that the *SSR* of the building complex can be higher than that of a single building, regardless of the battery capacity, battery distribution pattern, and converter loss, with a powerful complementarity effect. The results of *SCR* exhibit a variation pattern that is similar to that of *SSR*. The *SCR* of the distributed storage is higher than the corresponding reference value, and the difference decreases with increasing battery capacity. The *SCR* of centralized storage is higher than that of distributed storage and increases with the battery capacity. Moreover, it is apparent that *SSR* increases and *SCR* decreases without considering converter loss when comparing the result in Figure 9 and Tables 3 and 4.

Table 3. *SSR* comparison between distributed storage and centralized storage without considering converter loss.

Reference SSR	Cap_b of Distributed Storage			SSR	Cap_b of Centralized Storage	SSR
	Office	Apartment	Mall			
55%	0.070	0.316	0.058	55.14%	0.444	55.86%
60%	0.156	0.410	0.141	60.04%	0.707	60.77%
65%	0.249	0.520	0.237	65.02%	1.006	65.92%
70%	0.358	0.670	0.346	70.02%	1.374	71.32%
75%	0.553	0.994	0.568	75.01%	2.115	76.29%
80%	1.188	2.993	1.452	80.00%	5.633	81.51%

Table 4. *SCR* comparison between distributed storage and centralized storage without considering converter loss.

Reference SCR	Cap_b of Distributed Storage			SCR	Cap_b of Centralized Storage	SCR
	Office	Apartment	Mall			
55%	0.063	0.281	0.052	55.17%	0.396	55.83%
60%	0.139	0.361	0.126	60.05%	0.626	60.69%
65%	0.222	0.452	0.210	65.02%	0.884	65.75%
70%	0.313	0.558	0.302	70.02%	1.173	71.02%
75%	0.432	0.709	0.432	75.01%	1.573	76.18%
80%	0.746	1.046	0.782	80.01%	2.574	81.23%
85%	1.663	2.784	2.436	85.00%	6.883	86.51%

In summary, the existence of converter loss will reduce the *SSR* and increase the *SCR* of the system; the complementarity effect of load curves will increase both *SSR* and *SCR*; and the centralized storage scheme exhibits greater performance than distributed storage, regardless of whether the converter loss is considered.

4.2. Effect of PV Penetration

PV penetration is typically defined as the ratio of the total PV generation energy to the building load. The results in Section 3 are primarily aimed at the condition that the PV penetration value is 1. In this section, the effect of PV penetration on the building complex is analyzed. Table 5 lists the calculation indicators for different PV penetrations. When the PV penetration value is 1 or 1.5, the *SSR* of the centralized storage is higher than that of the optimal allocation scheme. When the PV penetration is 0.5, the *SSR* of the centralized storage is lower than that of the optimal allocation scheme, and the *SCR* for both distribution schemes is almost 100%. It indicates that for the PV penetration condition of 0.5, the major PV generation is directly consumed by the building load, and it is appropriate to store the remaining energy in the battery inside the building, not in the centralized battery storage, which will cause extra energy loss with the converter. The *SCR* of the centralized storage is always higher than the optimal allocation scheme for each PV penetration, with the influence of the complementarity effect and converter loss. In

summary, centralized storage shows better performance than distributed storage, except for some low PV penetration conditions.

Table 5. Evaluation indicators comparison of optimal allocation and centralized storage under different PV penetration and battery capacity *SSR* and *SCR* values.

PV Penetration	Cap_b	SSR		SCR	
		Optimal Allocation	Centralized Storage	Optimal Allocation	Centralized Storage
0.5	2	47.25%	47.11%	99.31%	99.81%
	4	47.62%	47.19%	99.99%	100%
	6	47.68%	47.19%	100%	100%
1	2	74.10%	74.75%	78.26%	80.23%
	4	78.73%	79.21%	83.24%	85.33%
	6	80.24%	80.64%	84.90%	87.08%
	8	81.20%	81.37%	85.98%	88.05%
	10	81.76%	81.81%	86.83%	88.70%
1.5	2	83.35%	84.51%	59.12%	60.98%
	4	89.30%	90.14%	63.41%	65.25%
	6	91.75%	92.54%	65.22%	67.13%
	8	93.35%	94.02%	66.42%	68.33%
	10	94.41%	95.09%	67.24%	69.23%

Table 6 lists the allocation ratios of the three buildings aimed at different optimization goals. When Cap_b is constant, the allocation ratio varies with PV penetration, and the variation does not show a distinct regularity. Hence, it is essential to consider the PV penetration and characteristics of the building load when selecting an appropriate allocation ratio in practical applications. In addition, the allocation ratio of the *SSR* optimization process is almost the same as the final allocation ratio for pursuing the maximal *SCR* under different PV penetrations and battery capacities. As mentioned in Section 3.2.1, the optimization directions of *SSR* and *SCR* are coincident in the distributed storage scheme.

Table 6. Allocation ratio for different optimization goals.

PV Penetration	Cap_b	Allocation Ratio (Optimization for SSR)			Allocation Ratio (Optimization for SCR)		
		Office	Apartment	Mall	Office	Apartment	Mall
0.5	2	30.0%	40.5%	29.5%	30.0%	40.5%	29.5%
	4	40.0%	30.5%	29.5%	40.0%	30.5%	29.5%
	6	39.0%	28.5%	32.5%	—	—	—
1	2	28.0%	43.0%	29.0%	28.0%	43.5%	28.5%
	4	35.0%	34.5%	30.5%	35.0%	35.5%	29.5%
	6	33.0%	36.0%	31.0%	33.0%	36.0%	31.0%
	8	33.0%	40.5%	26.5%	29.5%	41.5%	29.0%
	10	34.5%	36.5%	29.0%	31.5%	39.0%	29.5%
1.5	2	28.0%	44.0%	28.0%	28.0%	44.0%	28.0%
	4	33.5%	40.5%	26.0%	33.5%	40.5%	26.0%
	6	30.5%	39.5%	30.0%	30.5%	39.5%	30.0%
	8	31.5%	39.0%	29.5%	31.0%	39.0%	30.0%
	10	31.5%	40.0%	28.5%	30.0%	41.5%	28.5%

Figure 11 shows the *SSR* and *SCR* of centralized storage under different PV penetrations and battery capacities. When the PV penetration is constant, the *SSR* and *SCR* both increase with an increase in Cap_b. When Cap_b is constant, *SSR* increases with increasing PV penetration, and *SCR* decreases with increasing PV penetration. A contour line of 90% is shown in the figure. As shown in Figure 11, it is feasible to achieve a high *SSR* when the PV penetration is relatively high and achieve a high *SCR* when PV penetration

is relatively low for the centralized storage system. Hence, the configuration goal of the battery capacity can be determined based on the practical capacity of the PV installation. *SSR* should be recognized as an indicator of high PV penetration conditions, and *SCR* should be recognized as an indicator of low PV penetration conditions.
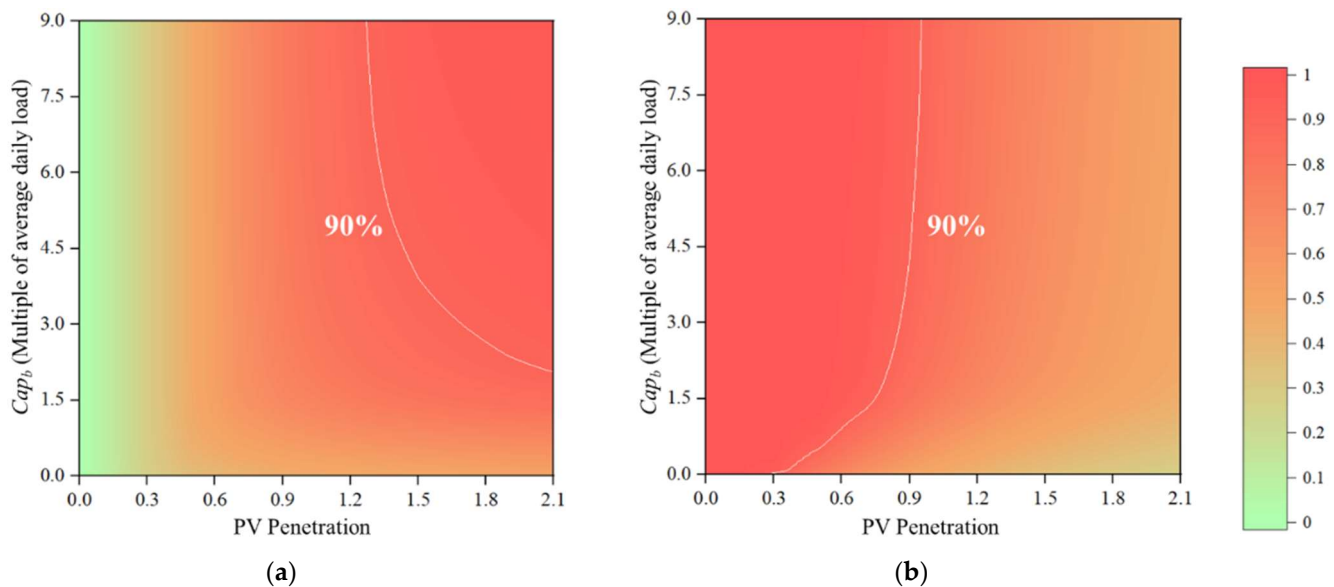

Figure 11. Effect of PV penetration and battery capacity for evaluation indicators with the centralized storage scheme: (**a**) *SSR*: (**b**) *SCR*.

4.3. Limitation and Outlook

The results presented in this study are subject to some limitations. The analysis of this study is based on the actual load data investigated from three kinds of buildings in Beijing, China. For the convenience of comparison, the load power time series of the three buildings are scaled to the same average daily electricity consumption of 100 kWh per day, which is different from the real energy consumption proportion. However, the nondimensionalization of load profiles, PV generation, and battery capacity make the simulation results universal. The performance of the PVB system in different PV installations is analyzed as an attempt to present the different relative sizes of PV capacity and building load. Furthermore, the battery capacity configuration method of the PVB system applied in a building complex proposed in this paper and the main conclusion are not limited by whether or not the actual load profile is adopted. The results and methodology relating to capacity configuration with the PVB system can be applied to large-scale building syntheses and used as a guide for battery capacity design in the PVB systems of building complexes. The efficiency of DC/DC in this study is adopted with the current device level. In the future, more efficient DC/DC will be manufactured and the energy conversion loss will be reduced in the PVB systems. However, the effects of converter loss and building load curve complementarity for building complexes are constant.

5. Conclusions

Battery storage is recognized as a powerful technique for enhancing the relative independence between a building PV system and utility grid. This paper presents a battery capacity configuration method for PVBs, aimed at improving the self-sufficiency and self-consumption of building complexes. In addition, the effects of converter loss and building load curve complementarity were analyzed. The main conclusions are as follows:

(1) The centralized storage scheme usually shows a greater system performance than a distributed storage scheme. The technical indicator *SSR* is more sensitive to the PV capacity than *SCR*. The *SCR* of centralized storage is consistently higher than

that of distributed storage for different battery capacities and PV penetrations. The *SSR* of centralized storage is only lower than that of distributed storage in the low PV penetration conditions when the converter loss dominates the benefits of centralized storage.

(2) There is a slight difference between the optimal allocation ratios achieved by the *SSR* and *SCR* considering that they have the same total battery capacity when equipped with a distributed storage scheme. The optimal allocation ratio for a building complex is determined based on the characteristics of a single building in the battery arrangement. The allocation ratios to achieve the maximal *SSR* under different battery and PV capacities are also tabulated. The *SCR* values of different combinations of battery and PV capacities are also shown.

(3) Converter loss decreases the *SSR* and increases the *SCR* of the PVB system in a building complex. The effect of complementarity in load curves and centralized batteries is conducive to increasing *SSR* and *SCR*, especially in the centralized storage scheme. The adoption of a high-efficiency converter can achieve a greater *SSR* for building complexes while reducing the battery capacity configuration.

Nomenclature

Greek symbols

α	A binary number
β	Installation angle of PV panels
γ	Temperature power coefficient ($1/^\circ$C)
η	Efficiency (%)
Δt	Time increment

Abbreviations

PV	Photovoltaic
PVB	Photovoltaic and battery
Cap	Capacity (kWh)
P	Power (kW)
NOCT	Nominal operating cell temperature ($^\circ$C)
T	Temperature ($^\circ$C)
SOC	State of charge
E	Total energy (kWh)
SSR	Self-sufficiency rate (%)
SCR	Self-consumption rate (%)

Subscripts

a	Ambient air
b	Battery
grid	Utility grid
load	Building load

dis	Discharge process of battery
ch	Charge process of battery
im	Electricity imported from the utility grid
ex	Electricity exported from the utility grid
max	Maximum
min	Minimum
Other variables	
I_t	Solar radiation intensity incident on PV panels (W/m^2)
I_{dir}	Direct solar radiation intensity on the horizontal plane (W/m^2)
I_{dif}	Diffuse solar radiation intensity on the horizontal plane (W/m^2)
I	Global solar radiation intensity on the horizontal plane (W/m^2)
$P_{PV,rated}$	Rated PV generation power (kW)
R_{dir}	Ratio of direct solar radiation on the inclined plane to the horizontal plane (%)

Appendix A

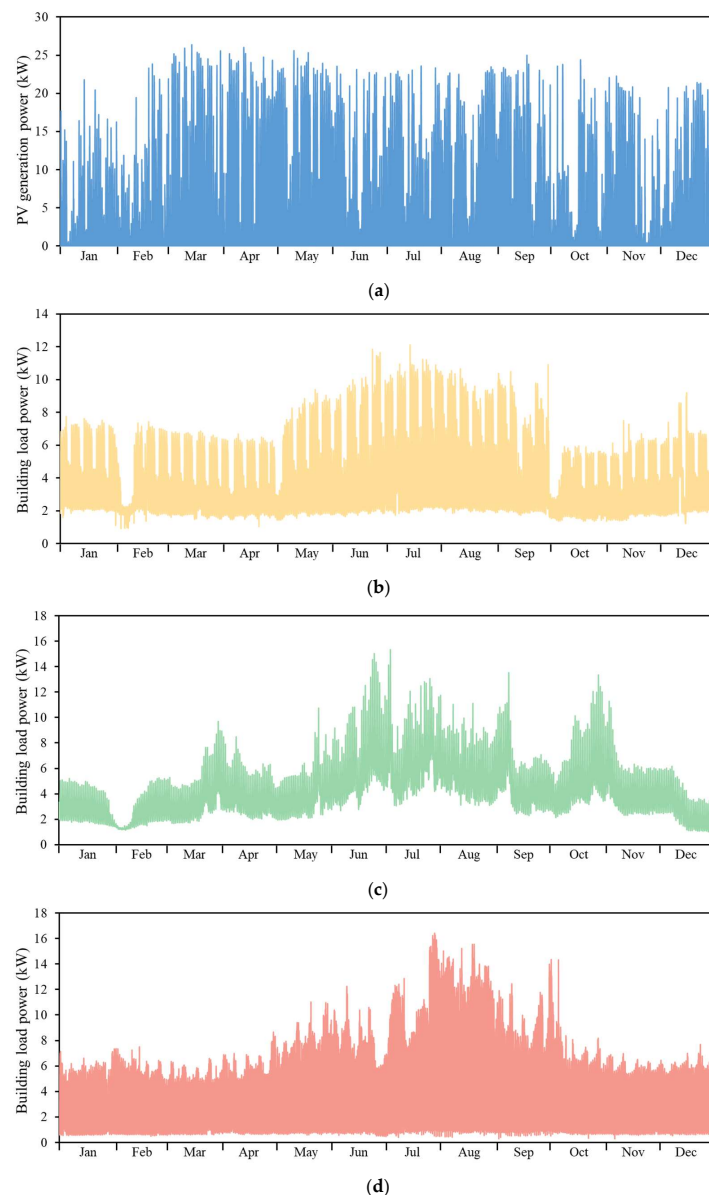Detailed time series PV generation and building load power data used in the study.

Figure A1. Annual power data: (**a**) PV generation; (**b**) office load; (**c**) apartment load; (**d**) mall load.

References

1. Chen, Q.; Kuang, Z.; Liu, X.; Zhang, T. Transforming a solar-rich county to an electricity producer: Solutions to the mismatch between demand and generation. *J. Clean. Prod.* **2022**, *336*, 130418. [CrossRef]
2. Khattak, S.I.; Ahmad, M.; Khan, Z.U.; Khan, A. Exploring the impact of innovation, renewable energy consumption, and income on CO2 emissions: New evidence from the BRICS economies. *Env. Sci. Pollut. Res. Int.* **2020**, *27*, 13866–13881. [CrossRef] [PubMed]
3. Jiang, Q.; Khattak, S.I.; Rahman, Z.U. Measuring the simultaneous effects of electricity consumption and production on carbon dioxide emissions (CO2e) in China: New evidence from an EKC-based assessment. *Energy* **2021**, *229*, 120616. [CrossRef]
4. Ahmed Ali, K.; Ahmad, M.I.; Yusup, Y. Issues, Impacts, and Mitigations of Carbon Dioxide Emissions in the Building Sector. *Sustainability* **2020**, *12*, 7427. [CrossRef]
5. Mishra, S.; Saini, G.; Saha, S.; Chauhan, A.; Kumar, A.; Maity, S. A survey on multi-criterion decision parameters, integration layout, storage technologies, sizing methodologies and control strategies for integrated renewable energy system. *Sustain. Energy Technol. Assess.* **2022**, *52*, 102246. [CrossRef]
6. Yang, J.; Yang, Z.; Duan, Y. Capacity optimization and feasibility assessment of solar-wind hybrid renewable energy systems in China. *J. Clean. Prod.* **2022**, *368*, 133139. [CrossRef]
7. Sharma, S.; Sengar, N. Review of solar PV training manuals and development of survey based solar PV system training formats for beginners. *Sol. Energy* **2022**, *241*, 72–84. [CrossRef]
8. Qiu, T.; Wang, L.; Lu, Y.; Zhang, M.; Qin, W.; Wang, S.; Wang, L. Potential assessment of photovoltaic power generation in China. *Renew. Sustain. Energy Rev.* **2022**, *154*, 111900. [CrossRef]
9. Stainsby, W.; Zimmerle, D.; Duggan, G.P. A method to estimate residential PV generation from net-metered load data and system install date. *Appl. Energy* **2020**, *267*, 114895. [CrossRef]
10. Gul, E.; Baldinelli, G.; Bartocci, P.; Bianchi, F.; Domenghini, P.; Cotana, F.; Wang, J. A techno-economic analysis of a solar PV and DC battery storage system for a community energy sharing. *Energy* **2022**, *244*, 123191. [CrossRef]
11. Gerber, D.L.; Vossos, V.; Feng, W.; Marnay, C.; Nordman, B.; Brown, R. A simulation-based efficiency comparison of AC and DC power distribution networks in commercial buildings. *Appl. Energy.* **2018**, *210*, 1167–1187. [CrossRef]
12. Ge, J.; Shen, C.; Zhao, K.; Lv, G. Energy production features of rooftop hybrid photovoltaic–wind system and matching analysis with building energy use. *Energy Convers. Manag.* **2022**, *258*, 15485. [CrossRef]
13. Zhang, K.; Prakash, A.; Paul, L.; Blum, D.; Alstone, P.; Zoellick, J.; Brown, R.; Pritoni, M. Model predictive control for demand flexibility: Real-world operation of a commercial building with photovoltaic and battery systems. *Adv. Appl. Energy* **2022**, *7*, 100099. [CrossRef]
14. Bird, L.; Lew, D.; Milligan, M.; Carlini, E.M.; Estanqueiro, A.; Flynn, D.; Gomez-Lazaro, E.; Holttinen, H.; Menemenlis, N.; Orths, A.; et al. Wind and solar energy curtailment: A review of international experience. *Renew. Sustain. Energy Rev.* **2016**, *65*, 577–586. [CrossRef]
15. Chaibi, Y.; Allouhi, A.; Salhi, M.; El-jouni, A. Annual performance analysis of different maximum power point tracking techniques used in photovoltaic systems. *Prot. Control Mod. Power Syst.* **2019**, *4*, 1–10. [CrossRef]
16. Zhu, Y.; Xu, X.; Yan, Z.; Lu, J. Data acquisition, power forecasting and coordinated dispatch of power systems with distributed PV power generation. *Electr. J.* **2022**, *35*, 107133. [CrossRef]
17. Hao, D.; Qi, L.; Tairab, A.M.; Ahmed, A.; Azam, A.; Luo, D.; Pan, Y.; Zhang, Z.; Yan, J. Solar energy harvesting technologies for PV self-powered applications: A comprehensive review. *Renew. Energy* **2022**, *188*, 678–697. [CrossRef]
18. Ma, T.; Zhang, Y.; Gu, W.; Xiao, G.; Yang, H.; Wang, S. Strategy comparison and techno-economic evaluation of a grid-connected photovoltaic-battery system. *Renew. Energy* **2022**, *197*, 1049–1060. [CrossRef]
19. Li, Y.; Peng, J.; Jia, H.; Zou, B.; Hao, B.; Ma, T.; Wang, X. Optimal battery schedule for grid-connected photovoltaic-battery systems of office buildings based on a dynamic programming algorithm. *J. Energy Storage* **2022**, *50*, 104557. [CrossRef]
20. Chellaswamy, C.; Ganesh Babu, R.; Vanathi, A. A framework for building energy management system with residence mounted photovoltaic. *Build. Simul.* **2021**, *14*, 1031–1046. [CrossRef]
21. Hesse, H.; Martins, R.; Musilek, P.; Naumann, M.; Truong, C.; Jossen, A. Economic Optimization of Component Sizing for Residential Battery Storage Systems. *Energies* **2017**, *10*, 835. [CrossRef]
22. Chang, L.; Ma, C.; Zhang, Y.; Li, H.; Xiao, L. Experimental assessment of the discharge characteristics of multi-type retired lithium-ion batteries in parallel for echelon utilization. *J. Energy Storage* **2022**, *55*, 105539. [CrossRef]
23. Khezri, R.; Mahmoudi, A.; Whaley, D. Optimal sizing and comparative analysis of rooftop PV and battery for grid-connected households with all-electric and gas-electricity utility. *Energy* **2022**, *251*, 123876. [CrossRef]
24. Argyrou, M.C.; Marouchos, C.C.; Kalogirou, S.A.; Christodoulides, P. A novel power management algorithm for a residential grid-connected PV system with battery-supercapacitor storage for increased self-consumption and self-sufficiency. *Energy Convers. Manag.* **2021**, *246*, 114671. [CrossRef]
25. Jiang, Y.; Kang, L.; Liu, Y. A unified model to optimize configuration of battery energy storage systems with multiple types of batteries. *Energy* **2019**, *176*, 552–560. [CrossRef]
26. Li, J.; Zhang, Z.; Shen, B.; Gao, Z.; Ma, D.; Yue, P.; Pan, J. The capacity allocation method of photovoltaic and energy storage hybrid system considering the whole life cycle. *J. Clean. Prod.* **2020**, *275*, 122902. [CrossRef]

27. Zou, B.; Peng, J.; Yin, R.; Li, H.; Li, S.; Yan, J.; Yang, H. Capacity configuration of distributed photovoltaic and battery system for office buildings considering uncertainties. *Appl. Energy* **2022**, *319*, 119243. [CrossRef]
28. Li, S.; Zhang, T.; Liu, X.; Xue, Z.; Liu, X. Performance investigation of a grid-connected system integrated photovoltaic, battery storage and electric vehicles: A case study for gymnasium building. *Energy Build.* **2022**, *270*, 112255. [CrossRef]
29. Mohamad, F.; Teh, J.; Lai, C.-M. Optimum allocation of battery energy storage systems for power grid enhanced with solar energy. *Energy* **2021**, *223*, 120105. [CrossRef]
30. Anuradha, K.B.J.; Jayatunga, U.; Perera, H.Y.R. Loss-Voltage Sensitivity Analysis Based Battery Energy Storage Systems Allocation and Distributed Generation Capacity Upgrade. *J. Energy Storage* **2021**, *36*, 102357. [CrossRef]
31. Su, D.; Lei, Z. Optimal configuration of battery energy storage system in primary frequency regulation. *Energy Reports.* **2021**, *7*, 157–162. [CrossRef]
32. Kusakana, K. Optimal energy management of a grid-connected dual-tracking photovoltaic system with battery storage: Case of a microbrewery under demand response. *Energy* **2020**, *212*, 102357. [CrossRef]
33. Paul Ayeng'o, S.; Axelsen, H.; Haberschusz, D.; Sauer, D.U. A model for direct-coupled PV systems with batteries depending on solar radiation, temperature and number of serial connected PV cells. *Sol. Energy* **2019**, *183*, 120–131. [CrossRef]